NACA RM L57D05

Superseded by
TND 955

NACA

RESEARCH MEMORANDUM

HEAT TRANSFER AND BOUNDARY-LAYER TRANSITION ON A HIGHLY POLISHED HEMISPHERE-CONE IN FREE FLIGHT AT MACH NUMBERS UP TO 3.14 AND REYNOLDS NUMBERS UP TO 24×10^6

By James J. Buglia

Langley Aeronautical Laboratory
Langley Field, Va.

NATIONAL ADVISORY COMMITTEE
FOR AERONAUTICS

WASHINGTON
April 18, 1957
Declassified January 12, 1961

NATIONAL ADVISORY COMMITTEE FOR AERONAUTICS

RESEARCH MEMORANDUM

HEAT TRANSFER AND BOUNDARY-LAYER TRANSITION ON A HIGHLY POLISHED HEMISPHERE-CONE IN FREE FLIGHT AT MACH NUMBERS UP TO 3.14 AND REYNOLDS NUMBERS UP TO 24×10^6

By James J. Buglia

SUMMARY

A highly polished hemisphere-cone having a ratio of nose radius to base radius of 0.74 and a half-angle of 14.5° was flight tested at Mach numbers up to 4.70. Temperature and pressure data were obtained at Mach numbers up to 3.14 and a free-stream Reynolds number of 24×10^6 based on body diameter. The nose of the model had a surface roughness of 2 to 5 microinches as measured with an interferometer. The measured Stanton numbers were in good agreement with theory. Transition Reynolds numbers based on the laminar boundary-layer momentum thickness at transition ranged from 2,190 to 794. Comparison with results from previous tests of blunt shapes having a surface roughness of 20 to 40 microinches showed that the high degree of polish was instrumental in delaying the transition from laminar to turbulent flow.

INTRODUCTION

Bodies having high drag-to-weight ratios have become very important in the design of long-range ballistic missiles. These missiles, upon reentering the earth's atmosphere, are subject to severe aerodynamic heating. If long runs of laminar flow can be maintained, the lower heating rates associated with laminar boundary layers ease the problem of designing the nose-metal heat sink.

For many years surface roughness has been believed to be an important factor in affecting the Reynolds number of transition from laminar to turbulent flow. Several investigators (refs. 1 to 3) have indicated definite trends in transition Reynolds number by relating the transition Reynolds number to a roughness factor which is a function of the roughness

height and the laminar boundary-layer thickness. Another factor which shows promise as a boundary-layer stability parameter is the Reynolds number based on the laminar boundary-layer momentum thickness. These investigations were conducted on slender bodies. Other free-flight slender-body tests have shown that relatively long runs of laminar flow (transition Reynolds numbers of about 35×10^6) could be obtained with surface finishes of the order of 25 to 50 microinches. The possible disastrous effects of roughness of this magnitude on transition on blunt bodies were not clearly pointed out, however. Initial rocket tests with large-scale blunt noses (refs. 4 and 5) vividly pointed out that with roughness of 25 to 50 microinches transition was likely to occur at Reynolds numbers as low as 1×10^6 to 2×10^6. It was conjectured that the very thin boundary layers associated with the blunt nose were far more susceptible to roughness effects than were the thicker boundary layers on the slender bodies.

The Langley Pilotless Aircraft Research Division has undertaken a program to investigate the heat transfer and boundary-layer transition on nose shapes giving promise of application to ballistic-type missiles. The highlights of some of these tests are presented in reference 5.

The present investigation deals with the heat transfer and boundary-layer transition on a large, blunt hemisphere-cone having a half-angle of 14.5°, a ratio of nose radius to base radius of 0.74, and a base diameter of 17.56 inches. The surface of the model had a mirror finish, with a surface roughness of 2 to 5 microinches. An attempt is made to determine the gross effects of roughness on transition.

Only the data between 7 and 8 seconds of flight are presented in this report in order to make these data available at the earliest possible date. This time period is representative of one during which both high Reynolds numbers and high Mach numbers were experienced. At later times, where higher values of these parameters were experienced, the data appeared to be erratic, indicating that the model may have suffered some type of partial failure.

The investigation was conducted at an angle of attack of 0° and covered a Mach number range from 2.32 to 3.14 and free-stream Reynolds numbers per foot ranging from 13.1×10^6 to 16.5×10^6. The flight test was conducted at the Langley Pilotless Aircraft Research Station at Wallops Island, Va.

SYMBOLS

c	specific heat of wall, Btu/lb-$^{\circ}$F
c_p	specific heat of air, Btu/slug-$^{\circ}$F
D	diameter of hemisphere, ft
$f(\theta)$	heating parameter
M	Mach number
N_{Pr}	Prandtl number
N_{St}	Stanton number
P	pressure coefficient, $\frac{p_v - p_\infty}{q_\infty}$
p	pressure, lb/sq ft
q	dynamic pressure, $\frac{\gamma}{2} p_\infty M_\infty^2$
$\dot{q}$	time rate of heat input, Btu/(sq ft)(sec)
R	Reynolds number
$R_{\theta,t}$	transition Reynolds number based on laminar boundary-layer momentum thickness
T	temperature, $^{\circ}$R
t	time, sec
V	velocity, ft/sec
w	density of wall material, lb/cu ft
x	surface distance from stagnation point, ft
γ	ratio of specific heats
ρ	density of air, slugs/cu ft
θ	angle measured from stagnation point, deg
τ	wall thickness, ft

Subscripts:

aw	adiabatic wall
s	stagnation conditions
v	local conditions
w	pertaining to wall
∞	free stream

MODEL

The model was propelled by a two-stage rocket combination. The booster stage was a standard Honest John rocket motor, designated JATO, 4-DS-105,000, M6, and the sustainer was a standard Nike booster rocket motor, designated JATO, 2.5-DS-59000, X216A2. The test section, the nose of the Nike, was a hemisphere-cone having a ratio of nose radius to base radius of 0.74 on a half-angle of 14.5°. Figures 1 and 2 show the model and booster on the launcher.

The nose of the model consisted of 0.032-inch Inconel, backed with a layer of 3/8-inch balsa, mounted on a 3/8-inch magnesium casting. The balsa was used to support the Inconel and to minimize heat loss due to conduction. The balsa was removed by an undercut 1.5 inches wide and 1/8 inch deep extending along the thermocouple line. Pressure tubes were welded to the Inconel skin. The surface of the nose was highly polished to a roughness of 2 to 3 microinches on the hemispherical portion of the nose, and 3 to 5 microinches on the conical portion, as measured with an interferometer. Figure 3 shows a closeup of the nose, from which the degree of polish can be realized.

The booster fins were a set of standard fins for the Honest John rocket motor, $7\frac{1}{2}$ square feet per panel. The sustainer fins were magnesium castings. A sheet of 0.032-inch Inconel was wrapped around the leading edges of the sustainer fins, extending about 5 inches back from the leading edge and fastened to the magnesium. This sheet was then wrapped with a second sheet of 0.050-inch Inconel which extended back 1 inch from the leading edge. This increase in leading-edge radius and mass near the leading edge was necessary to prevent failure of the fins by aerodynamic heating, which caused structural failure in earlier models of this type. Ground tests were conducted in a high-temperature jet on a full-scale model of the outboard portion of the fin, where the heating to the fins was adjusted to simulate flight conditions. These tests indicated that

the Inconel wrappings would protect the load-bearing magnesium structure. Figure 4 shows the fin with the Inconel wrappings. Reference 6 describes the fin design, construction, and testing in greater detail.

INSTRUMENTATION AND TESTS

Skin temperatures along the nose were telemetered during the flight to a ground receiving station by using 12 chromel-alumel thermocouples welded to the inner surface of the skin and located as shown in figure 5. These measurements were commutated during flight at such a rate that every measurement was sampled at about every 0.1 second. Pressures were measured at six stations along a ray 180° from the thermocouple line. These are also shown in figure 5. Longitudinal accelerations were measured by thrust and drag accelerometers. Atmospheric and wind conditions were measured by radiosonde balloons launched near the time of flight and tracked with a Rawin set AN/GMD-1A. Velocity data were obtained by means of CW Doppler radar, and altitude and flight-path data were measured with an NACA modified SCR-584 space radar.

The model was launched from a zero-length launcher at an elevation angle of 55°. The Honest John booster accelerated the model to a Mach number of 2.23. After the booster thrust was expended, the booster drag separated and the model coasted for about 1.7 seconds. The Nike sustainer then fired and accelerated the model to its peak Mach number of 4.70, approximately 9.85 seconds after take-off. Free-stream temperature, pressure, and density related to model flight time are shown in figure 6, and free-stream Mach number and Reynolds number per foot are plotted against time in figure 7.

DATA REDUCTION

The temperature measurements from this test were reduced to dimensionless Stanton numbers by using the standard thin-wall formula

$$N_{St,\infty} = \frac{cw\tau}{c_p \rho_\infty V_\infty} \frac{\frac{dT_w}{dt}}{(T_{aw} - T_w)}$$

Radiation and conduction effects were estimated and found to be negligible for the times for which data are presented. The adiabatic wall temperature was calculated from the definition of recovery factor

$$\text{Recovery factor} = \frac{T_{aw} - T_v}{T_{s,\infty} - T_v}$$

where the recovery factor was assumed to be equal to its turbulent value of $N_{Pr}^{1/3}$ based on wall temperature. This assumption is obviously not correct for the stagnation point, where the recovery factor is equal to unity, and for the stations and times where laminar flow existed. The forcing function $T_{aw} - T_w$ is large enough, however, that the use of $N_{Pr}^{1/3}$ introduces a negligible error in the present results.

In order to check the validity of using the thin-wall equation in reducing the measured temperature data, the temperature lag through the skin was calculated by a method developed by P. R. Hill of the Langley Pilotless Aircraft Research Division and was found to be of the order of 10° or less and was thus considered negligible, as this value is well within the expected range of accuracy of the thermocouples, which was $\pm 24^{\circ}$.

Newtonian theory, modified as suggested in reference 7, was used to determine the pressure distribution and, hence, the local conditions over the nose. Previous experiments (for example, refs. 7 and 8) indicate that, even at the relatively low Mach numbers of this test, the modified Newtonian theory closely predicts the pressure distribution over a hemisphere. The pressure over the conical portion of the nose was assumed to be equal to that on the hemisphere at the juncture of the hemisphere and the cone. Calculations were made to ascertain the validity of using the modified Newtonian theory to determine the local conditions, rather than the measured pressures. These calculations were performed for the station just ahead of the juncture where the difference between the measured and calculated pressure coefficients was the greatest. It was found that the difference between the calculated and measured values of $\rho_v V_v$ was less than 8 percent, which is within the probable accuracy of the Stanton numbers presented. Thus, for the sake of simplicity and expediency in the data-reducing procedures, the modified Newtonian theory was used to determine the local conditions. As a matter of interest, however, a plot of the measured and calculated pressure coefficients is given as a function of surface length from the stagnation point in figure 8.

THEORETICAL CALCULATIONS

Laminar Heat Transfer

The laminar heat transfer over the hemispherical portion of the nose was evaluated from the theory of reference 9. This reference gives the following equations for the ratio of the rate of heat transfer to any point on the hemisphere to the heat transfer to the stagnation point:

$$\frac{\dot{q}}{\dot{q}_s} = \frac{2\theta \sin\theta \left[\left(1 - \frac{1}{\gamma M_\infty^2}\right)\cos^2\theta + \frac{1}{\gamma M_\infty^2}\right]}{\left[f(\theta)\right]^{1/2}}$$

where

$$f(\theta) = \left(1 - \frac{1}{\gamma M_\infty^2}\right)\left(\theta^2 - \frac{\theta \sin 4\theta}{2} + \frac{1 - \cos 4\theta}{8}\right) +$$

$$\frac{4}{\gamma M_\infty^2}\left(\theta^2 - \theta \sin 2\theta + \frac{1 - \cos 2\theta}{2}\right)$$

The ratio of Stanton numbers then becomes

$$\frac{N_{St,\infty}}{(N_{St,\infty})_s} = \frac{\dot{q}}{\dot{q}_s}\frac{(T_{aw} - T_w)_s}{(T_{aw} - T_w)}$$

where the forcing functions are evaluated from measured data. The values of $(N_{St,\infty})_s$ were calculated by the theory of reference 10.

Over the conical portion of the nose the measurements are compared with values calculated by the flat-plate theory of reference 11. Experience has shown that for a very blunt cone the flat-plate theory shows better agreement with experiment than does cone theory.

Turbulent Heat Transfer

No attempt was made to calculate the turbulent heating over the hemispherical portion of the nose. Over the conical portion, however, the flat-plate theory of reference 12 was used, modified as suggested in reference 13. The length used in the Reynolds number was the surface length from the stagnation point to the point in question. The modification of reference 13 consisted of using the factor 0.6 instead of 0.5 in the Reynolds analogy.

RESULTS AND DISCUSSION

The wall temperatures at each station for the first 8 seconds of flight are shown in figure 9. Shortly after 8 seconds the data became erratic. It was conjectured that deformation of the nose of the model changed the local flow conditions, and the data received after that time were considered to be unreliable.

The results of the heating analysis are presented in figure 10. The heating parameter is given as Stanton number based on free-stream conditions. Also shown are the local Reynolds number and the ratio of wall temperature to local static temperature.

Examination of figure 10(a) shows that at this time (t = 7.0 seconds) the flow is laminar over the entire nose, with the exception of the last station, which is in transition. If the assumption is made that transition takes place just ahead of the last station, the local transition Reynolds number is about 15×10^6. From the method given by appendix B of reference 14, the Reynolds number of transition based on the laminar boundary-layer momentum thickness at the transition point is 2,170. Figures 10(b) to 10(f) show similar data except that the transition point moves forward with increasing free-stream Mach number. It is of interest to note that the flow rearward of the transition point is not fully turbulent, as far back as the measurements were made. This flow is transitional until 8 seconds, when fully developed turbulent flow appears. The Reynolds numbers of transition based on momentum thickness were 2,190, 1,318, 794, 798, and 804 at times of 7.2, 7.4, 7.6, 7.8, and 8.0 seconds, respectively. References 4 and 5 report transition Reynolds numbers based on momentum thickness ranging from about 450 to 220 for about the same Mach number range as the present investigation. The model of reference 4 was a hemisphere-cylinder, and the highlights of an investigation on a nose shape similar to the one reported herein are given in reference 5. This model was a hemisphere-cone having a ratio of nose radius to base radius of 0.5 as compared with 0.74 for the model of this test. The models of references 4 and 5 had a roughness of 25 to 30 microinches. Comparison of the momentum thickness Reynolds numbers of transition of these tests with those of the present investigation shows that the high polish applied to the model appreciably delayed transition.

CONCLUDING REMARKS

A highly polished hemisphere-cone model was flight tested at Mach numbers up to 3.14 and at free-stream Reynolds numbers up to 24×10^6 based on diameter. The surface roughness was 2 to 5 microinches as

measured with an interferometer. Reynolds numbers of transition based on the laminar boundary-layer momentum thickness at the transition point of the present investigation ranged from 2,190 to 794 as compared with momentum transition Reynolds numbers of 450 to 220 for similar nose shapes of standard roughness (20 to 30 microinches) for the same Mach number range. It was concluded that the high polish greatly delayed transition. Existing theory adequately predicted both laminar and turbulent heating rates over the conical portion of the nose and laminar rates over the hemispherical portion. No attempt was made to predict the turbulent heating over the hemispherical portion of the nose.

Langley Aeronautical Laboratory,
National Advisory Committee for Aeronautics,
Langley Field, Va., March 27, 1957.

REFERENCES

1. Seiff, Alvin: A Review of Recent Information on Boundary-Layer Transition at Supersonic Speeds. NACA RM A55L21, 1956.

2. Low, George M.: Boundary-Layer Transition at Supersonic Speeds. NACA RM E56E10, 1956.

3. Czarnecki, K. R., and Sinclair, A. R.: Factors Affecting Transition at Supersonic Speeds. NACA RM L53I18a, 1953.

4. Garland, Benjamine J., and Chauvin, Leo T.: Measurements of Heat Transfer and Boundary-Layer Transition on an 8-Inch-Diameter Hemisphere Cylinder in Free Flight for a Mach Number Range of 2.00 to 3.88. NACA RM L57D04a, 1957.

5. Chauvin, Leo T.: Aerodynamic Heating of Aircraft Components. NACA RM L55L19b, 1956.

6. Bland, William B., Jr., and Bressette, Walter E.: Some Effects of Heat Transfer at Mach Number 2.0 at Stagnation Temperatures Between 2,310° and 3,500° R on a Magnesium Fin With Several Leading-Edge Modifications. NACA RM L57C14, 1957.

7. Oliver, Robert E.: An Experimental Investigation of Flow Over Simple Blunt Bodies at a Nominal Mach Number of 5.8. GALCIT Memo. No. 26 (Contract No. DA-04-495-Ord-19), June 1, 1955.

8. Chauvin, Leo T.: Pressure Distribution and Pressure Drag for a Hemispherical Nose at Mach Numbers of 2.05, 2.54, and 3.04. NACA RM L52K06, 1952.

9. Lees, Lester: Laminar Heat Transfer Over Blunt-Nosed Bodies at Supersonic Flight Speeds. Jet Propulsion, vol. 26, no. 4, Apr. 1956, pp. 259-269.

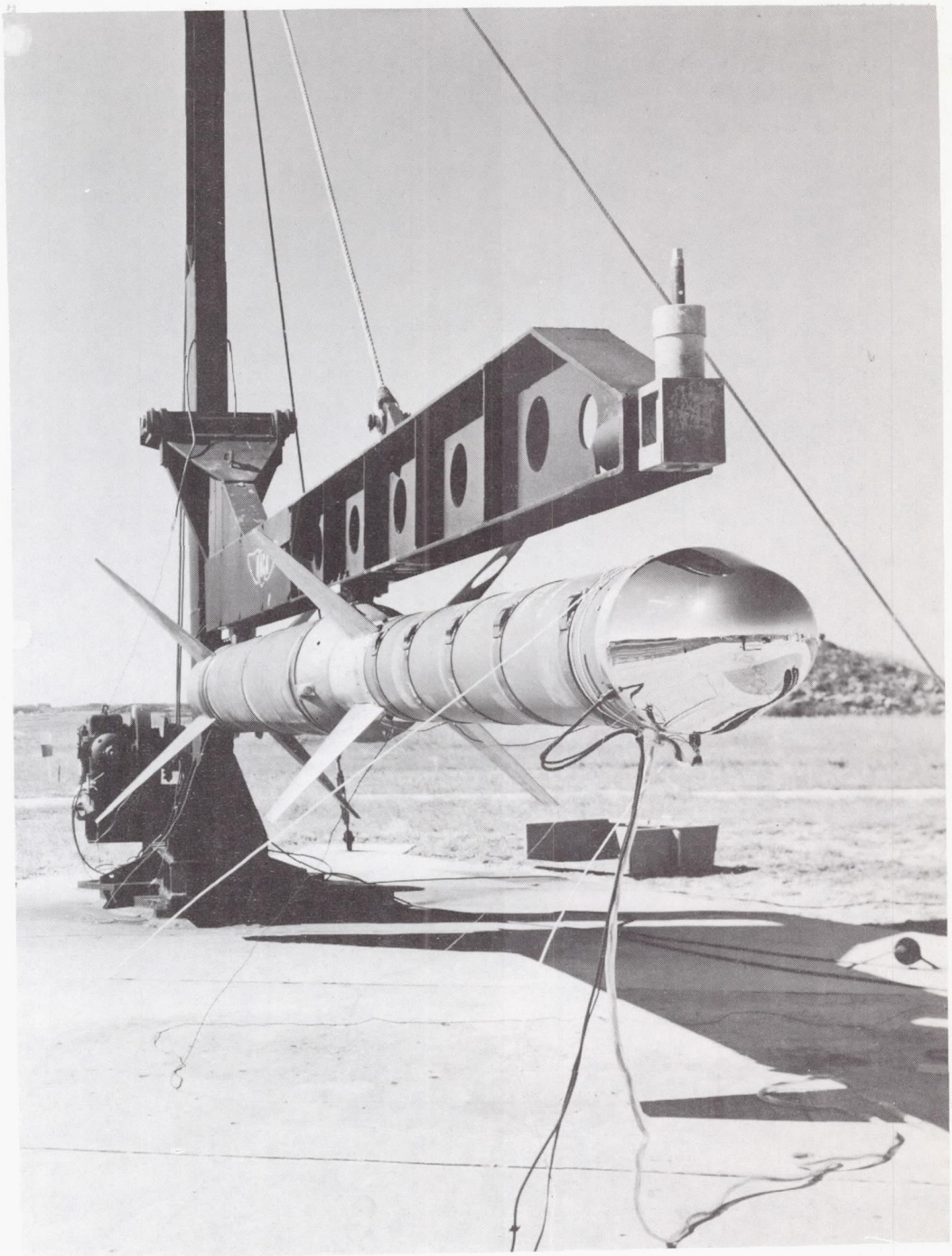
10. Sibulkin, M.: Heat Transfer Near the Forward Stagnation Point of a Body of Revolution. Jour. Aero. Sci. (Readers' Forum), vol. 19, no. 8, Aug. 1952, pp. 570-571.

11. Van Driest, E. R.: Investigation of Laminar Boundary Layer in Compressible Fluids Using the Crocco Method. NACA TN 2597, 1952.

12. Van Driest, E. R.: Turbulent Boundary Layer in Compressible Fluids. Jour. Aero. Sci., vol. 18, no. 3, Mar. 1951, pp. 145-160, 216.

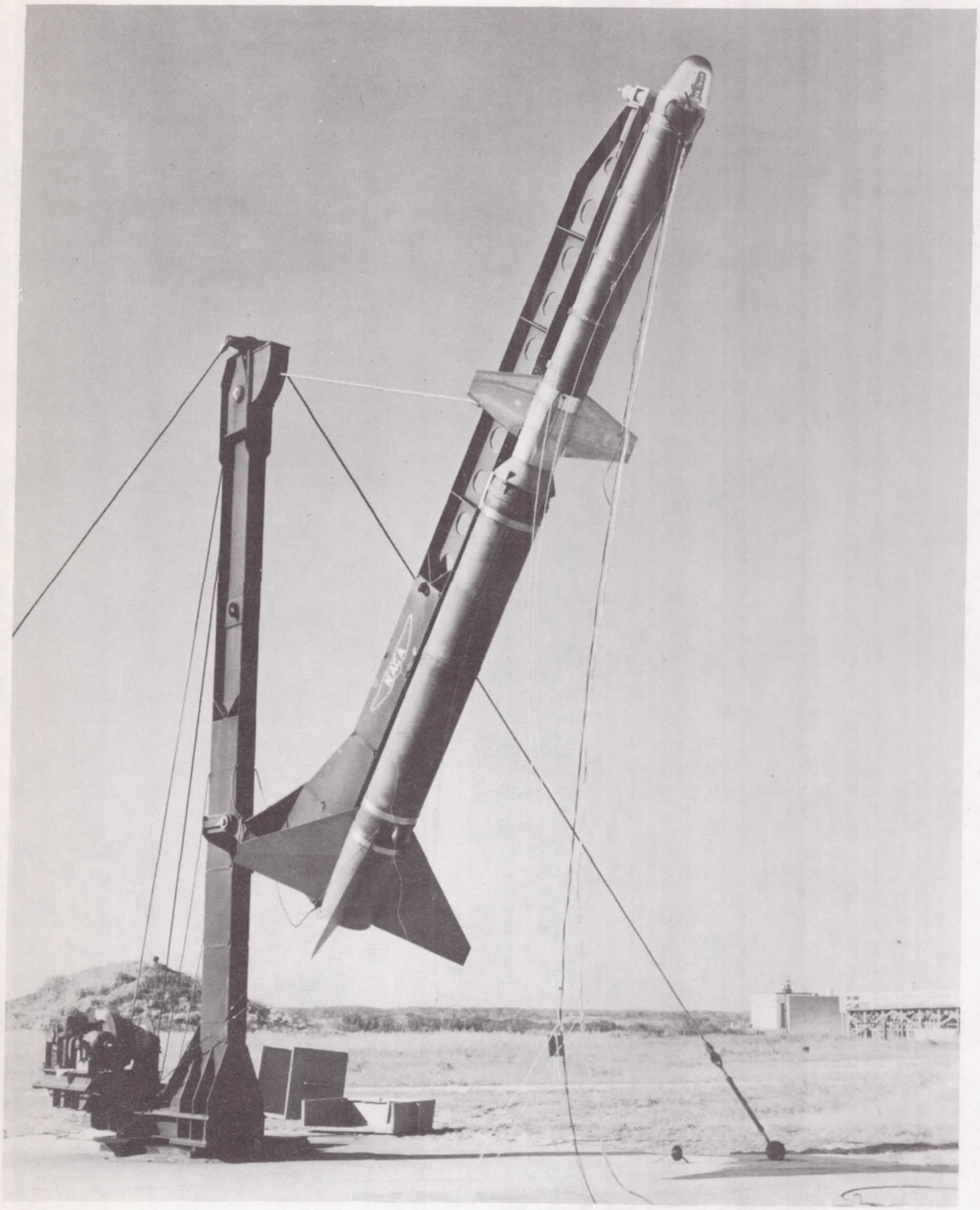
13. Rubesin, Morris W.: A Modified Reynolds Analogy for the Compressible Turbulent Boundary Layer on a Flat Plate. NACA TN 2917, 1953.

14. X-17 Re-Entry Test Vehicle - R-1 Final Flight Report. Rep. No. MSD-1834 (Contract No. AF 04(645)-7), Lockheed Aircraft Corp., July 17, 1956.



L-96362

Figure 1.- Photograph of model and booster on launcher.



L-96360

Figure 2.- Photograph of model and booster in launching position.

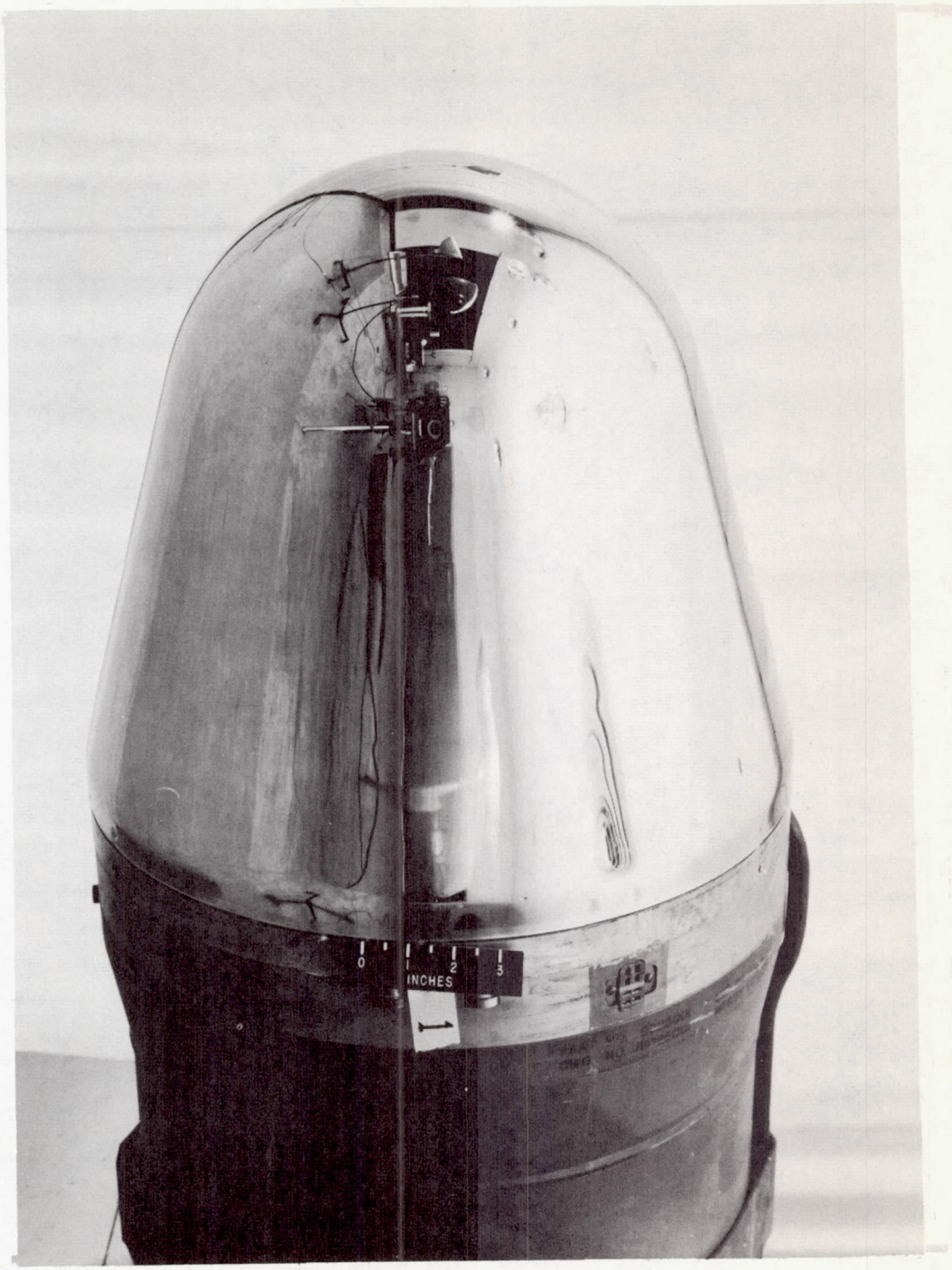
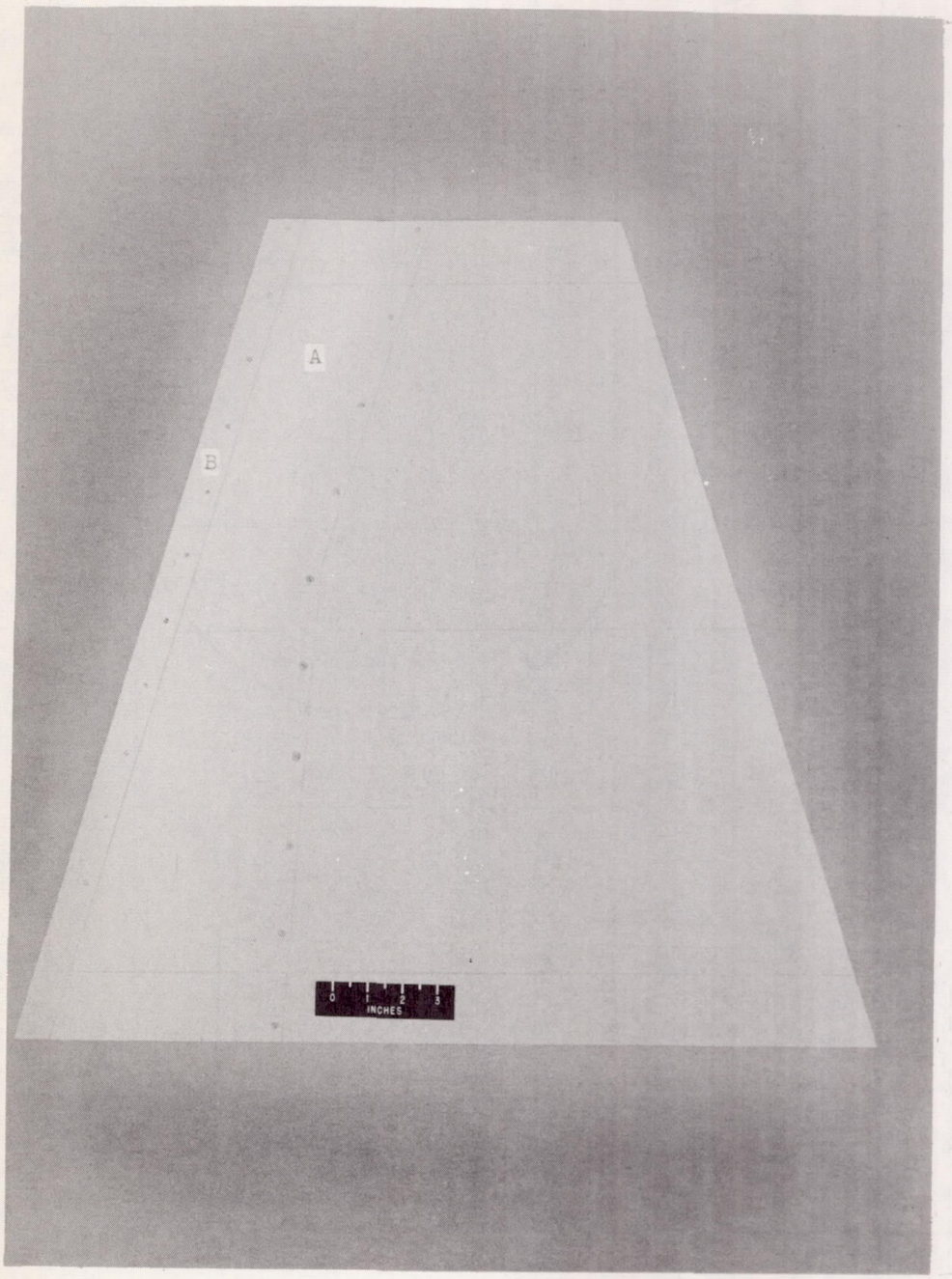


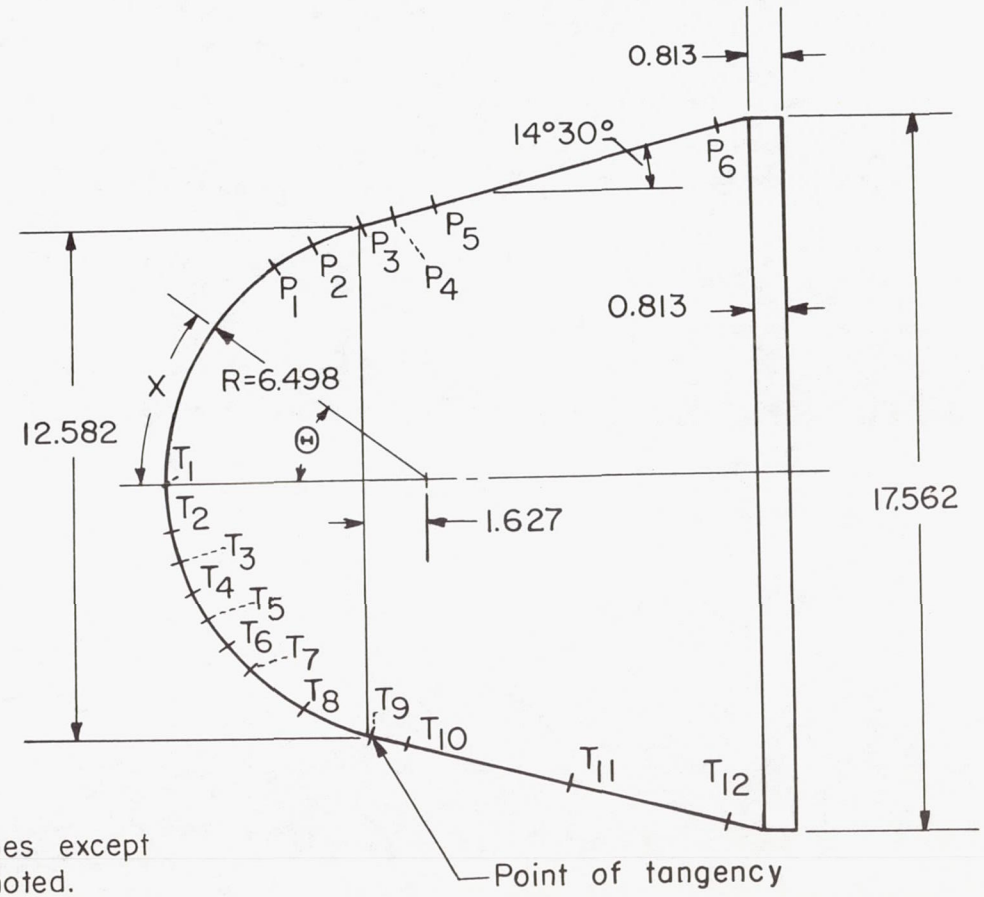
Figure 3.- Close-up of nose showing high degree of polish. L-96346



L-96341.1

Figure 4.- Photograph of fin showing construction details of leading edge. First and second Inconel caps are represented by A and B, respectively.

Pickup	θ, deg	x, in.
P_1	55	6.23
P_2	65	7.37
P_3	76	8.62
P_4		9.72
P_5		10.84
P_6		17.81
T_1	0	0
T_2	10	1.13
T_3	17	1.93
T_4	24	2.72
T_5	31	3.52
T_6	38	4.31
T_7	45	5.10
T_8	60	6.81
T_9	76	8.62
T_{10}		10.64
T_{11}		13.64
T_{12}		18.34



All dimensions are in inches except where otherwise noted.

Figure 5.- Sketch of nose showing location of temperature and pressure pickup stations.

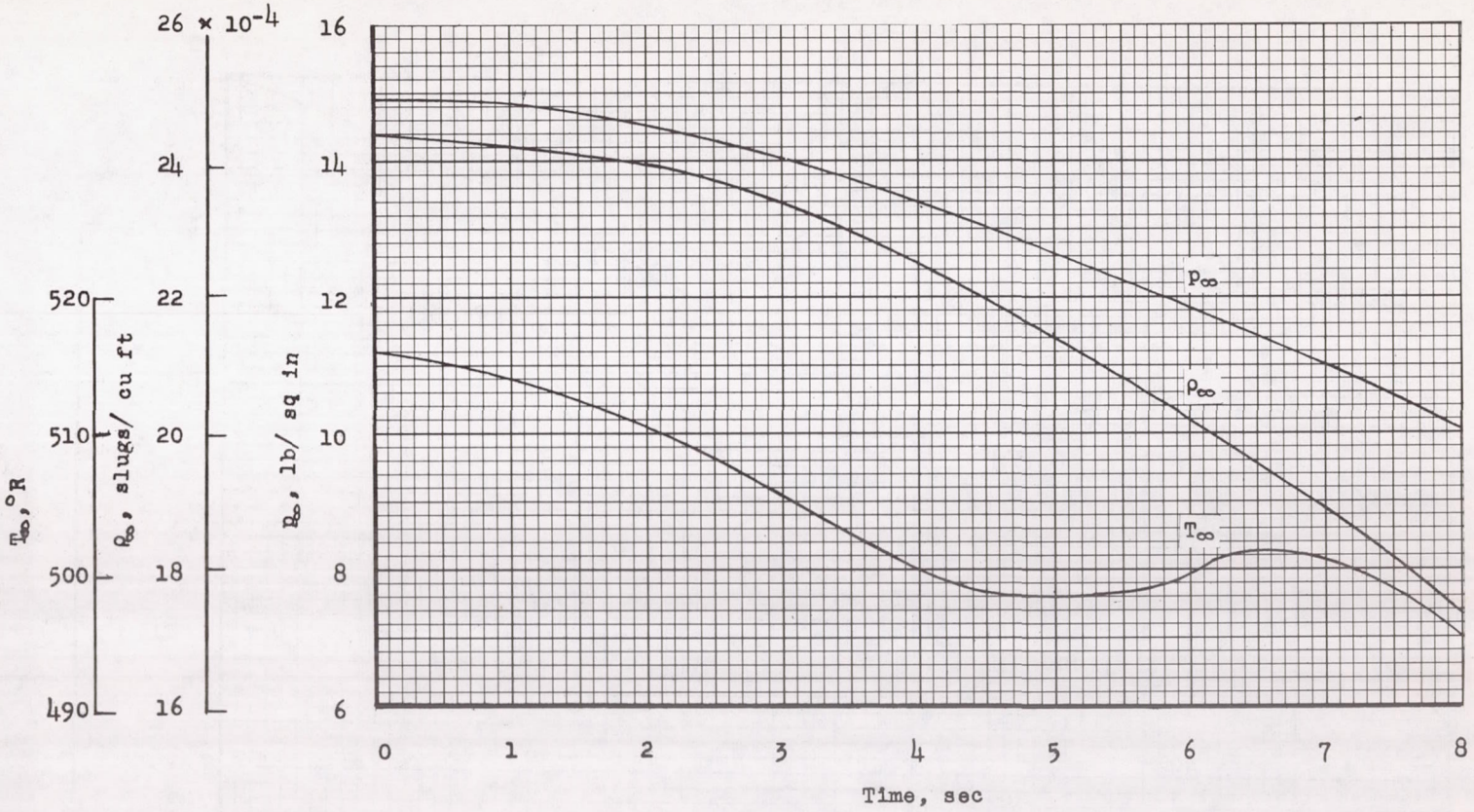


Figure 6.- Free-stream conditions related to model flight time.

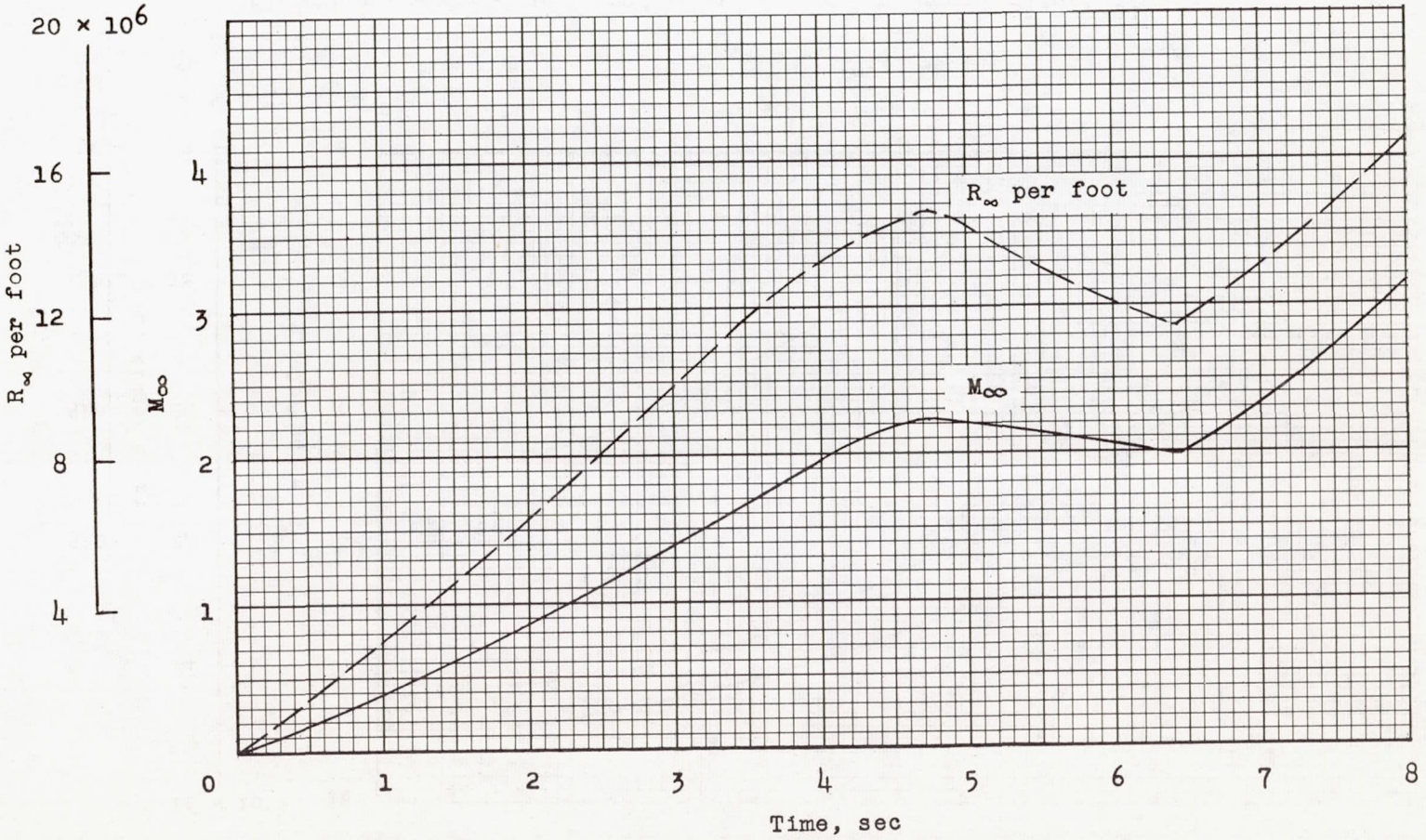


Figure 7.- Free-stream Mach number and Reynolds number per foot.

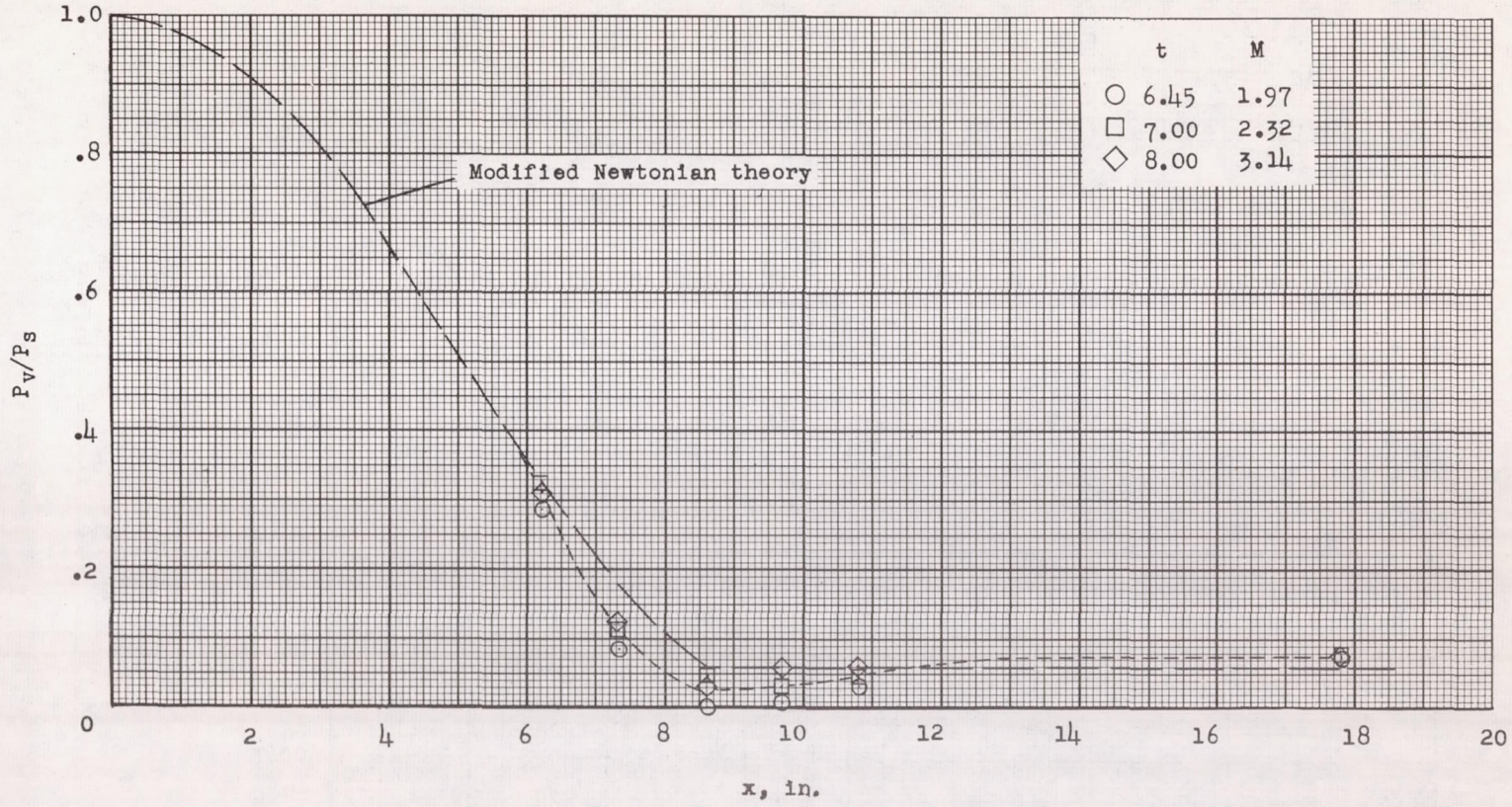


Figure 8.- Ratio of local to stagnation-point pressure coefficient.

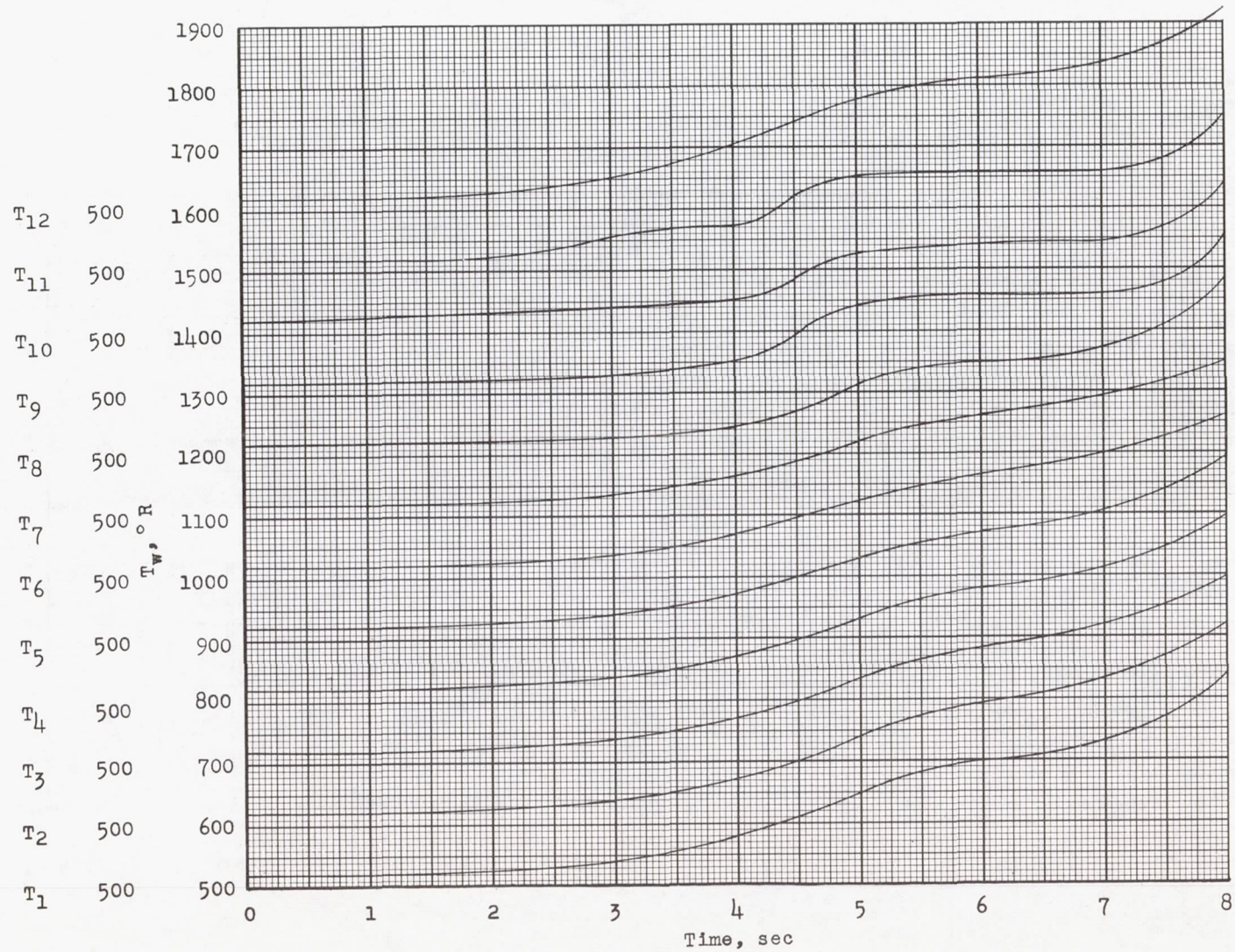
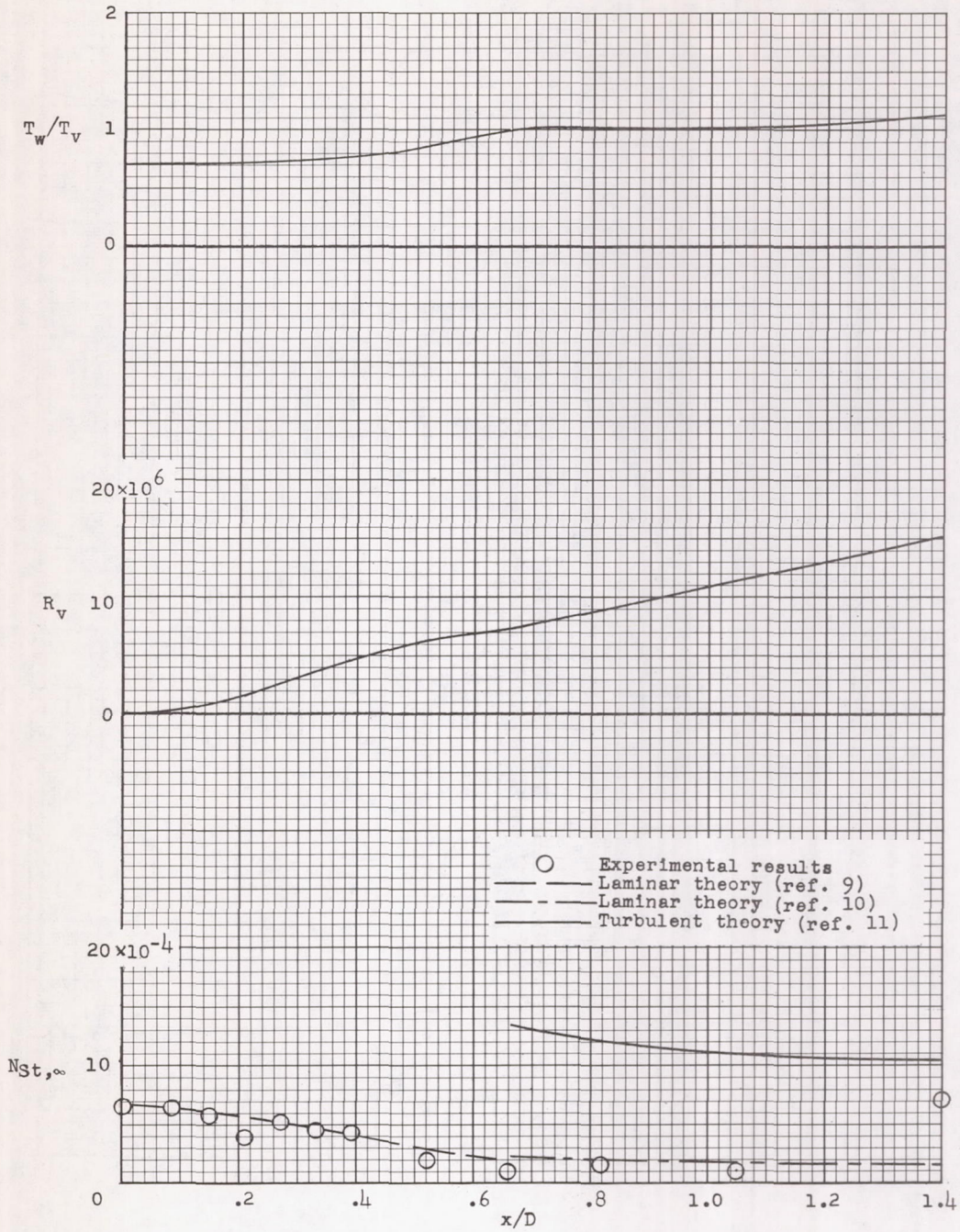
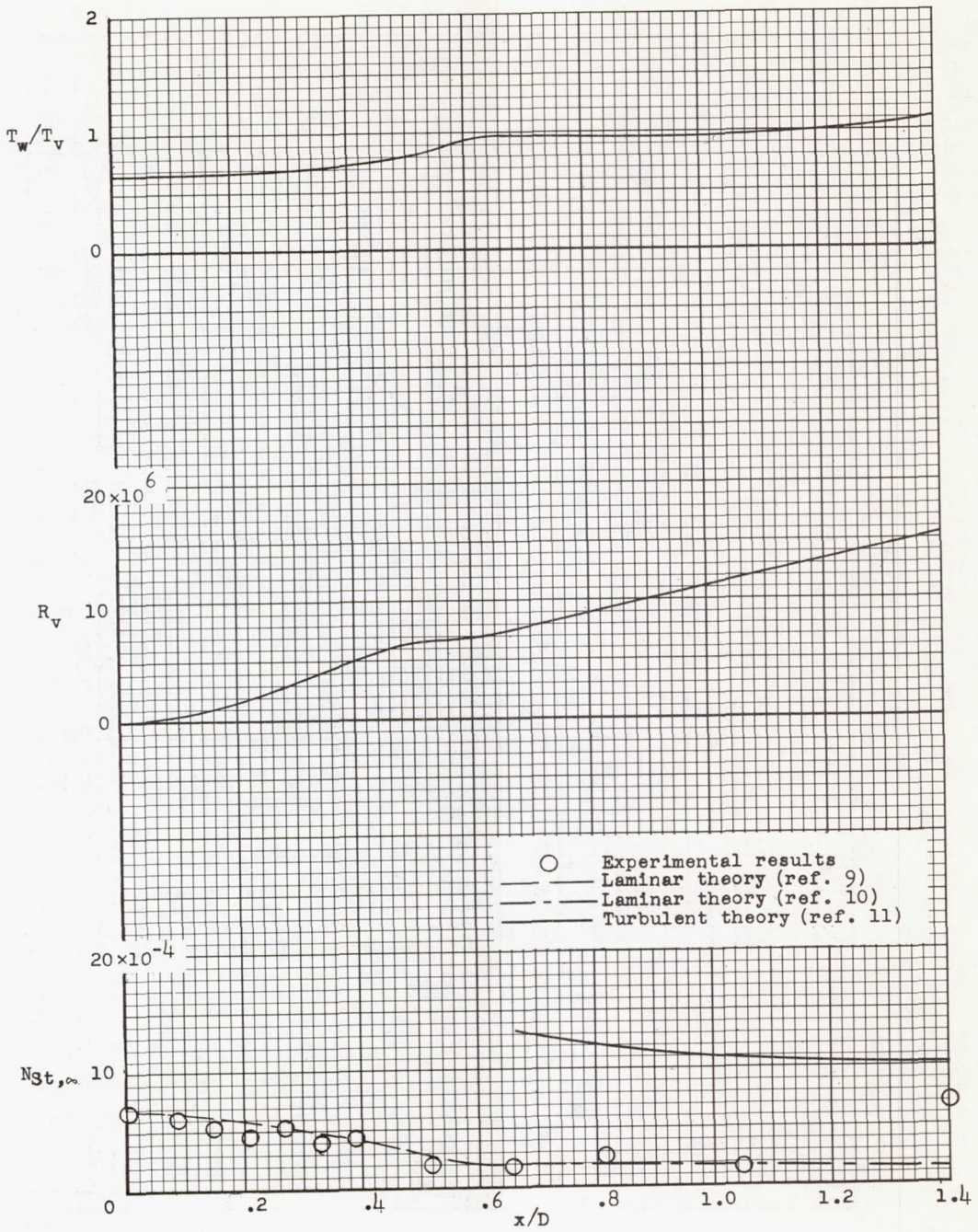


Figure 9.- Time histories of measured wall temperatures.



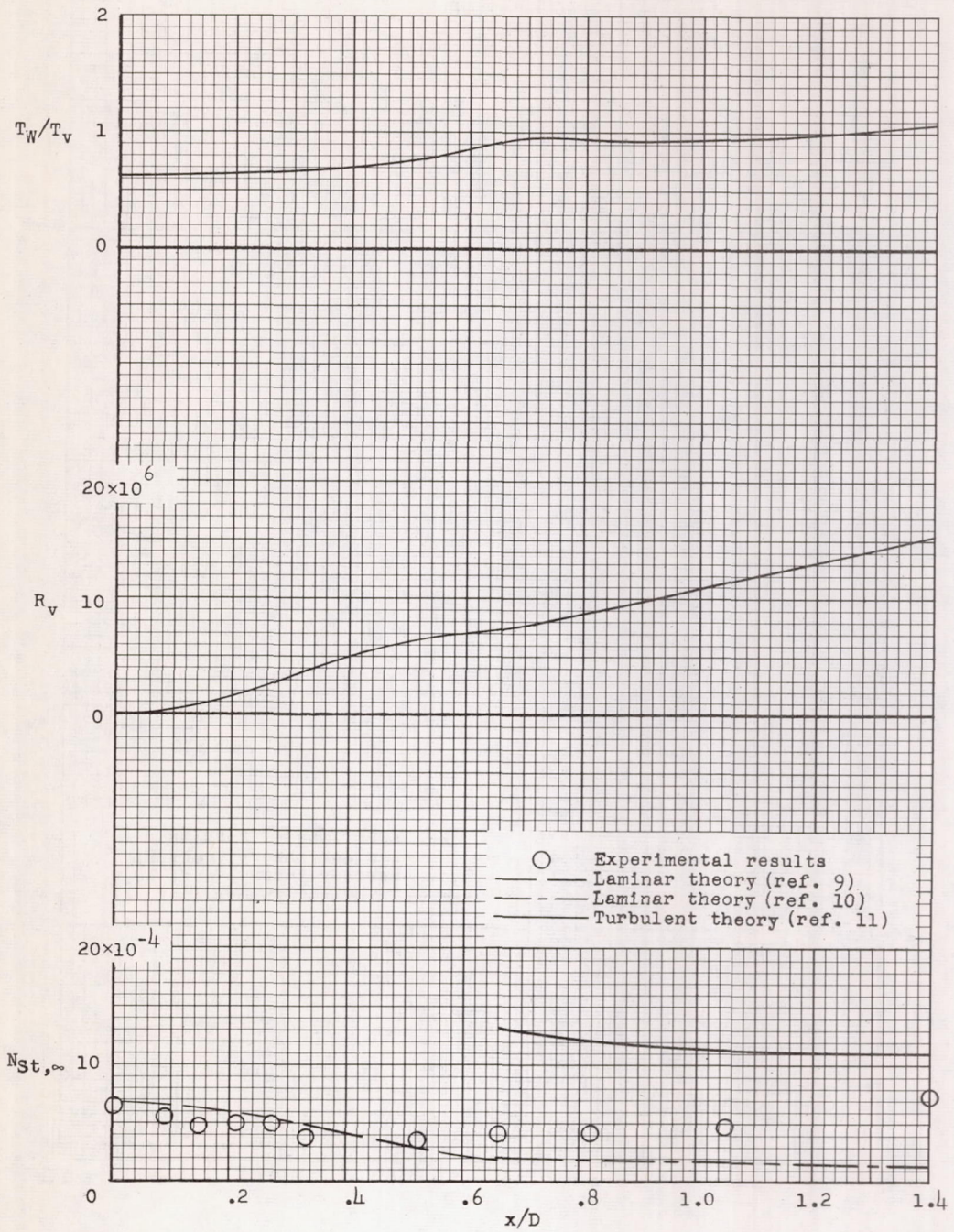
(a) $t = 7.0$ seconds; $M_\infty = 2.32$; $R_\infty = 13.1 \times 10^6$ per foot; $R_{\theta,t} = 2{,}170$.

Figure 10.- Free-stream Stanton numbers and pertinant local conditions.



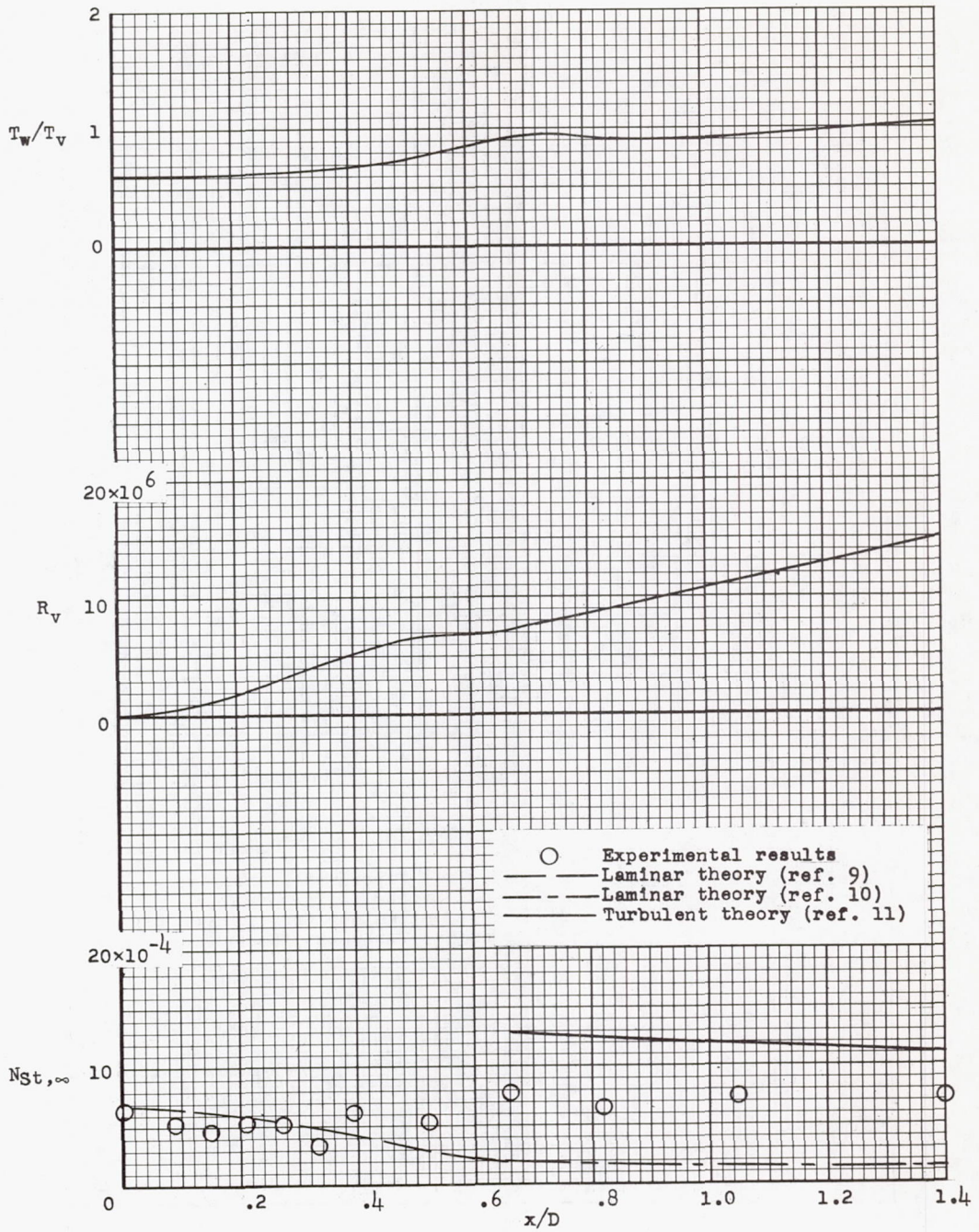
(b) $t = 7.2$ seconds; $M_\infty = 2.47$; $R_\infty = 13.8 \times 10^6$ per foot; $R_{\theta,t} = 2{,}190$.

Figure 10.- Continued.



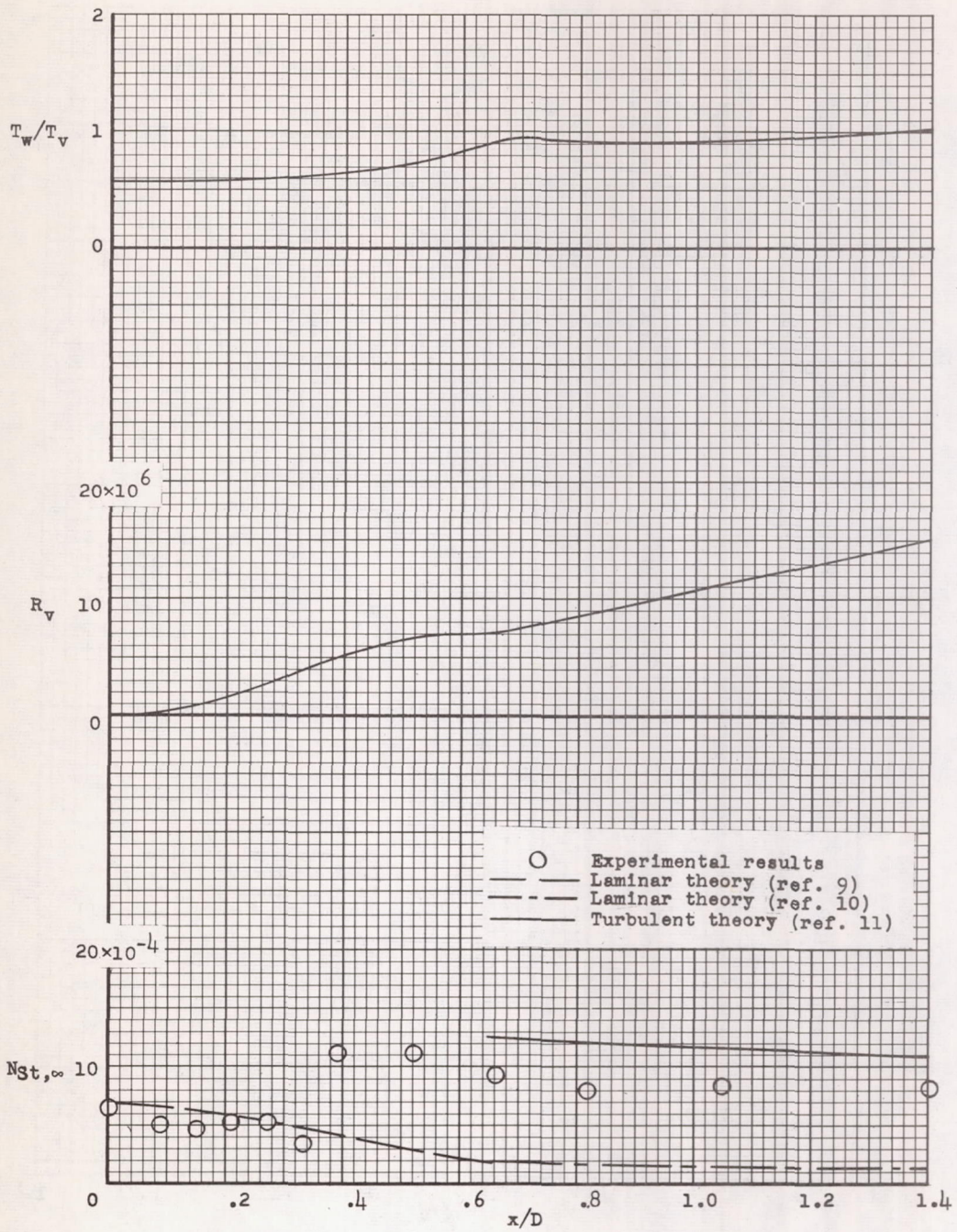
(c) $t = 7.4$ seconds; $M_\infty = 2.63$; $R_\infty = 14.5 \times 10^6$ per foot; $R_{\theta,t} = 1{,}318$.

Figure 10.- Continued.



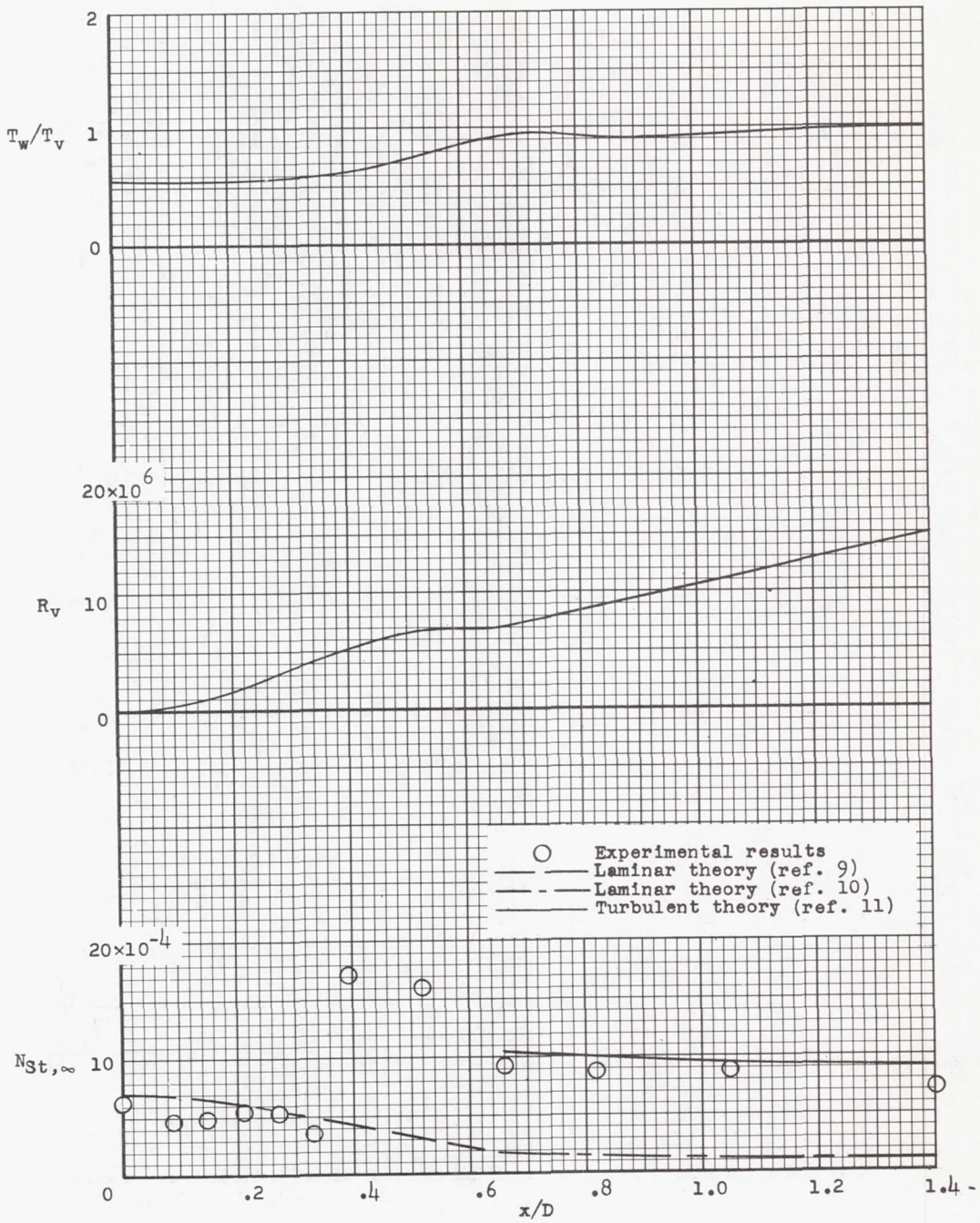
(d) $t = 7.6$ seconds; $M_\infty = 2.80$; $R_\infty = 15.2 \times 10^6$ per foot; $R_{\theta,t} = 794$.

Figure 10.- Continued.



(e) $t = 7.8$ seconds; $M_\infty = 2.97$; $R_\infty = 15.9 \times 10^6$ per foot; $R_{\theta,t} = 798$.

Figure 10.- Continued.



(f) $t = 8.0$ seconds; $M_\infty = 3.14$; $R_\infty = 16.5 \times 10^6$ per foot; $R_{\theta,t} = 804$.

Figure 10.- Concluded.